J. Mech. Phys. Solids 202 (2025) 106193

Contents lists available at ScienceDirect

Journal of the Mechanics and Physics of Solids

journal homepage: www.elsevier.com/locate/jmps

Entropic pressure on a confined biological vesicle with surface tension

Rubayet Hassan [a], Mingze Cai [b], Anh Vo [a], Samaneh Farokhirad [a], Xin Yan [b,*], Fatemeh Ahmadpoor [a,*]

[a] Department of Mechanical and Industrial Engineering, New Jersey Institute of Technology, Newark, NJ 07114, United States
[b] School of Mechanical Engineering and Automation, Beihang University, Beijing 100191, People's Republic of China

ARTICLE INFO

Keywords:
Thermal fluctuations
Statistical mechanics
Biological membranes
Entropic pressure

ABSTRACT

Entropic forces play a critical role in the dynamics and stability of soft matter systems, particularly in biological membranes and vesicles. The origin of these forces lies in the significant thermal fluctuations of soft membranes, a subject that has intrigued the scientific community for decades. Most studies focus on a simplified version of the problem: a flat, tensionless membrane, rather than more complex non-planar surfaces with pre-existing curvature and surface tension. In this paper, we revisit this problem for confined biological vesicles using statistical mechanics analysis and coarse-grained molecular dynamics simulations, explicitly incorporating their curvature field and surface tension. The coupling between the deformation field and the non-zero curvature field leads to a renormalized surface tension, significantly altering the entropic force compared to that of a planar membrane. We demonstrate that while the entropic pressure p follows a similar power-law behavior to that of a planar membrane at small distances, $p \propto 1/d^3$, it transitions to an exponential decay at larger distances. These findings provide insights into the coupled effects of surface tension, membrane configuration, and thermal fluctuations, particularly for understanding biological processes, such as vesicle fusion, endocytosis, and membrane-mediated interactions in crowded cellular environments.

1. Introduction

Biological vesicles are enclosed structures that are formed primarily by lipid bilayers that encapsulate various substances, including proteins, ions, and other molecules (Papahadjopoulos and Kimelberg, 1974; Yáñez-Mó et al., 2015). These vesicles are found throughout nature and are essential to many biological functions. Examples such as exosomes (Kalluri and LeBleu, 2020) and endosomes (Van Niel et al., 2018) facilitate the transport of molecules both within and between cells. Their structural stability allows them to protect their cargo from degradation, enabling safe fusion with cellular membranes, an important process in neurotransmitter release (Südhof, 2013), immune responses (Robbins and Morelli, 2014), and hormone signaling (Yamanaka et al., 2015). In biomedicine, synthetic vesicles, such as multi-lamellar liposomes, are engineered for drug delivery, where their stability is crucial to ensure the drug reaches its target without premature release (Gruner et al., 1985; Sharma and Sharma, 1997; Sun et al., 2021). From a mechanical perspective, vesicles are modeled as elastic shells with low bending rigidity, causing them to fluctuate significantly at physiological temperatures. These fluctuations influence vesicles' interactions with their surrounding bioenvironment. Processes such as exo- and endocytosis, vesicle fusion, pore formation, cell adhesion, binding–unbinding transitions, self-assembly, vesicle size

* Corresponding authors.
E-mail addresses: yan_xin@buaa.edu.cn (X. Yan), fatemeh.ahmadpoor@njit.edu (F. Ahmadpoor).

https://doi.org/10.1016/j.jmps.2025.106193
Received 28 January 2025; Received in revised form 13 April 2025; Accepted 13 May 2025
Available online 31 May 2025

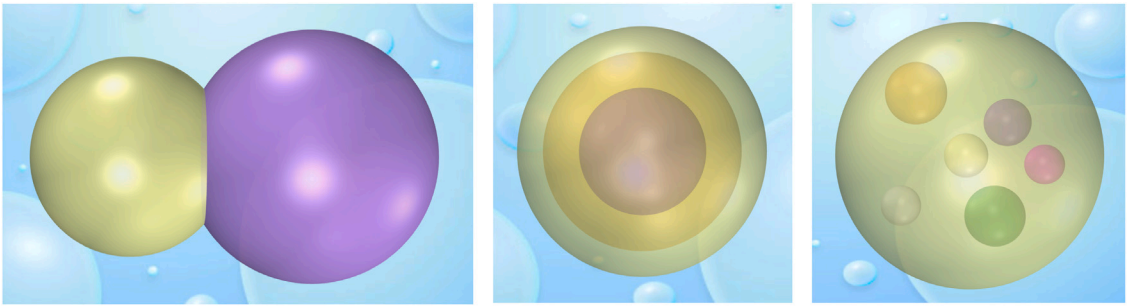

Fig. 1. Thermal fluctuations and entropic forces play a pivotal role in controlling vesicle fusion (left) and are also essential for the behavior and stability of multilamellar vesicles (MLVs) (middle) and multivesicular vesicles (MVs) (right).

distributions, and the configuration of red blood cell membranes are all affected by these fluctuations (Lipowsky and Seifert, 1991; Lipowsky and Leibler, 1986; Lee et al., 2010; Weikl and Lipowsky, 2004; Chen et al., 2008; Gao et al., 2005; Ahmadpoor and Sharma, 2016a,b; Gov et al., 2003; Dearnley et al., 2016; Kusters et al., 2019; Farokhirad et al., 2019, 2021; Mamun and Farokhirad, 2024). During interactions, membrane fluctuations are often confined and suppressed by nearby objects, such as other vesicles, substrates, viruses, or drug carriers. This confinement generates a so-called entropic force, a repulsive force that tends to push the other object away. This entropic pressure was first addressed in the context of cell–cell interactions by Helfrich (1978) and subsequently examined by several groups in both the physics (Bachmann et al., 2001; Kleinert, 1999) and mechanics communities (Freund, 2013; Sharma, 2013; Hanlumyuang et al., 2014; Liang and Purohit, 2018; Mozaffari et al., 2021; Hassan et al., 2024; Chen and Kulkarni, 2015, 2017).

From the mechanics point of view, a closed fluctuating membrane is modeled as a fluid elastic sheet with bending deformations, and the energy associated with these deformations are well-described by the Helfrich energy (Helfrich, 1973)[1]:

$$U_b = \int \left[\frac{1}{2}\kappa_b H^2\right] dS. \tag{1}$$

Here κ_b is the membrane's bending modulus and H is the mean curvature. Note that in this model it is assumed that the surface tension of the membrane is negligible. Based on this assumption, Helfrich (1978) proposed that the entropic force between two fluctuating planar membranes at distance d should scale as $1/d^3$. Later, this power law has been verified in other theoretical and computational models (Bachmann et al., 2001; Hanlumyuang et al., 2014; Ahmadpoor et al., 2022).

Although biological membranes are often modeled as flat, tensionless elastic sheets, many cells and organelles have non-planar shapes and exhibit surface tension. Flat membranes can form oval or spherical vesicles involved in critical processes such as endocytosis, intracellular trafficking, and viral infection. These vesicles vary widely in size and lamellarity, adapting them for diverse applications. In all these cases, the assumption of a flat, tensionless membrane in the statistical mechanics model is clearly flawed due to the presence of finite curvature. On a curved surface, the out-of-plane fluctuations are coupled with the existing curvature field, resulting in an *effective surface tension* (Morse and Milner, 1995; Seifert, 1997; Lipowsky, 1991) that may be positive or negative depending on the vesicle's curvature and mechanical properties. In addition, unlike flat membranes, the vesicles cannot be stable without surface tension. According to the well-known Laplace law $p = 2\sigma/r_0^2$ (Laplace, 1806), the surface tension σ of the membrane must balance the hydrostatic pressure p to ensure the stability of the vesicle with radius r_0. The statistical mechanics of a single fluctuating spherical vesicle has been extensively investigated, with studies addressing topics including but not limited to size distribution (Ahmadpoor and Sharma, 2016b; Huang et al., 2017), active membranes (Turlier and Betz, 2018; Kulkarni, 2023; Ramesh and Kulkarni, 2024), effective surface tension (Loubet et al., 2012; Lipowsky, 1991), and nonlinear elasticity (Helfrich, 1986). However, the impact of these fluctuations on the entropic interactions between fluctuating vesicles and their surrounding bioenvironment remains unexplored (see Fig. 1). In this paper, we revisit the statistical mechanics of membrane fluctuations for a spherical vesicle in close proximity to another object—such as a neighboring vesicle, a virus, or a cell. Our focus is on developing both theoretical and computational frameworks to explore the nature of the entropic force that arises near a fluctuating curved surface. In particular, we investigate how this force depends on the membrane's curvature and the effective surface tension, which emerges from the interplay between out-of-plane fluctuations and the curvature field. In Section 2, we formulate a statistical mechanics model for a fluctuating vesicle under uniform confinement, akin to conditions observed in multilamellar vesicles. The entropic pressure is then derived in Section 3 for both small and large separations between the vesicle and the confining surface. In Section 4, we validate our theoretical predictions using coarse-grained molecular dynamics simulations of a fluid membrane and verify the corresponding scaling laws for the entropic force in the presence of surface tension. We conclude with a summary and discussion in Section 5.

[1] The original form not only includes the mean curvature, but also the Gaussian curvature with additional material constant known as Gaussian modulus.

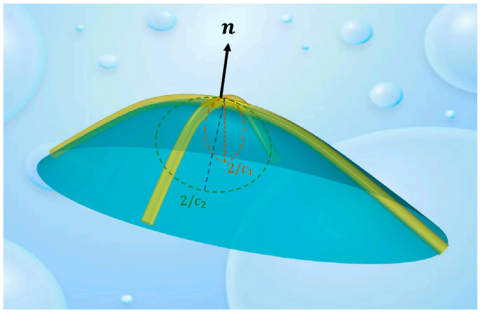

Fig. 2. Schematic of a surface bending deformation. The curvature at a point on the surface can be calculated in any direction. The principal curvatures c_1 and c_2 are the maximum and minimum of the curvature at a given point and are the invariants of the curvature tensor (Abbena et al., 2006). The mean curvature H, can be then obtained as $2H = c_1 + c_2 = -\mathrm{div}_S\mathbf{n}$, where $\mathbf{n}$ is the normal vector to the surface.

2. Statistical mechanics of a confined fluctuating vesicle

The elastic energy for the deformation of a fluid membrane can be described as:

$$F_e = \int_S \left[\frac{1}{2}\kappa_b H^2 + \kappa_G K + \sigma\right] J\, dS, \tag{2}$$

where κ_b and κ_G are the bending and Gaussian moduli, H and K are the mean and Gaussian curvatures, J is the Jacobian of the deformed surface, and σ is the surface tension of the membrane. Let $\mathbf{n}$ be the normal vector on the deformed surface S as shown in Fig. 2. The curvature tensor is defined as

$$\mathbf{L} = -\nabla_S\mathbf{n},$$

where ∇_S is the surface gradient operator[2](Biria et al., 2013). Then the mean H and Gaussian K curvatures are derived as Biria et al. (2013):

$$H = \frac{1}{2}\mathrm{tr}(\mathbf{L}) = -\frac{1}{2}\mathrm{div}_S\mathbf{n}, \quad K = \frac{1}{2}\left((\mathrm{tr}(\mathbf{L}))^2 - \mathrm{tr}(\mathbf{L}^2)\right),$$

where div_S and tr denote the surface gradient operator and trace of the tensor, respectively. We assume that the topology of the membrane does not change during deformations due to the thermal fluctuations and thus, according to the Gauss–Bonnet theorem (Abbena et al., 2006) the contribution of the Gaussian curvature to the free energy change will be neglected.

Now consider a closed vesicle of radius r_0 described by an enclosed surface $S := \{\mathbf{r} \in \mathbb{R}^3 : |\mathbf{r}| = r_0\}$ located inside a larger radius sphere R_0 as depicted in Fig. 3. The coordinates of a point on the vesicle surface are described by its polar and azimuthal angles (θ, ϕ). We assume that the displacement field on the vesicle surface is only along the normal direction and $U(\theta,\phi) : S \to \mathbb{R}$ denotes the magnitude of the out-of-plane displacement. Then the radius, mean curvature (H) and the Jacobian (J) of the deformed surface at any point can be expressed as:

$$\begin{aligned}
&\tilde{\mathbf{r}} = \mathbf{r} + U\mathbf{n},\\
&H = -\frac{1}{r_0} + \frac{U}{r_0^2} + \frac{1}{2}\Delta_S U - \frac{U\Delta_S U}{r_0} + \frac{1}{2r_0}\nabla_S U\cdot\nabla_S U - \frac{U^2}{r_0^3} + O(U^3)\\
&J = 1 + \frac{2U}{r_0} + \frac{1}{2}|\nabla_S U|^2 + \frac{U^2}{r_0^2} + O(U^3)
\end{aligned} \tag{3}$$

where Δ_S is the surface Laplacian operator (Biria et al., 2013). Substituting Eq. (3) in the elastic energy (2), and expanding up to the quadratic order we have:

$$F_e = \int_S \left[\frac{1}{2}\kappa_b\left(1 - \frac{1}{2}|\nabla_S U|^2 + U\Delta_S U + \frac{1}{4}r_0^2(\Delta_S U)^2\right) + \sigma\left(r_0^2 + \frac{1}{2}r_0^2|\nabla_S U|^2 + U^2\right)\right] d\Omega$$

[2] Let $\mathbf{n}$ be the normal vector to the surface $\mathbb{S}$. A surface projection tensor may be defined as:

$$\mathbf{P} = \mathbf{I} - \mathbf{n}\otimes\mathbf{n},$$

where $\mathbf{I}$ is the identity tensor. The surface gradient, surface Laplacian and surface divergence of a scalar field f and a vector field $\mathbf{g}$ can then be defined in terms of $\mathbf{P}$ and their smooth extensions f^e and $\mathbf{g}^e$ as Biria et al. (2013):

$$\nabla_S f = \mathbf{P}\nabla f^e, \qquad \nabla_S\mathbf{g} = (\nabla\mathbf{g}^e)\mathbf{P},$$
$$\mathrm{div}_S\mathbf{g} = \mathbf{P}\cdot\nabla\mathbf{g}^e, \qquad \Delta_S f = \mathrm{div}_S(\nabla_S f).$$

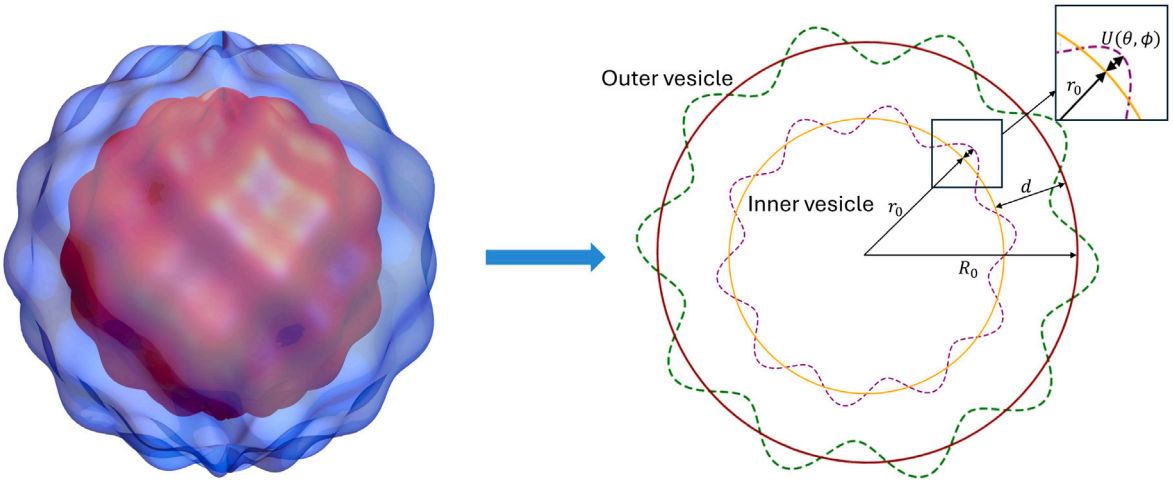

Fig. 3. The inner vesicle of radius r_0 is confined by outer vesicle of Radius R_0 within a confined distance $d = R_0 - r_0$. The fluctuating mid-plane displacement is normalized as $u(\theta,\phi) = U(\theta,\phi)/r_0$.

$$= \psi_e + \int_S \left[\frac{1}{2}\kappa_b\left(\frac{1}{4}r_0^2(\Delta_S U)^2 + \frac{3}{2}U\Delta_S U\right) + \sigma\left(U^2 - \frac{1}{2}r_0^2 U\Delta_S U\right)\right] d\Omega \tag{4}$$

where $d\Omega = \sin\theta d\theta d\phi$ and $\psi_e = 2\pi\kappa_b + 4\pi r_0^2\sigma$ is a constant term of no consequences. Following (Mozaffari et al., 2021; Ahmadpoor et al., 2022; Hassan et al., 2024), to capture the effect of confinement on the out-of-plane deformations, we introduce a quadratic potential function to penalize the larger fluctuations:

$$F_f = \int_S \frac{1}{2}\gamma_d U^2 d\Omega \tag{5}$$

Normalizing U with respect to the mean radius r_0 by defining a dimensionless variable $u = U/r_0$, we can expand the total energy F^{tot} as follows (Helfrich, 1986; Ahmadpoor and Sharma, 2016b):

$$F^{tot} = \int_S \left[\frac{1}{2}\kappa_b\left(\frac{1}{4}(\underline{\Delta}u)^2 + \frac{3}{2}u\underline{\Delta}u\right) + \sigma r_0^2\left(u^2 - \frac{1}{2}u\underline{\Delta}u\right) + \frac{1}{2}\gamma_d u^2\right] d\Omega \tag{6}$$

where $\underline{\Delta}$ is the normalized surface Laplacian operator in spherical coordinates.[3] Further, γ_d is introduced as a parameter, whose magnitude depends on the confinement, i.e. $d = R_0 - r_0$.

To study the fluctuations and free energy of the vesicle, we start by discretizing the normalized displacement field u using spherical harmonics. Let N be the total number of degrees of freedom and

$$\mathcal{K}_N := \{(l,m)|(l,m) \in \mathbf{Z}\times\mathbf{Z}, l \geqslant 2, l(l+1) < N, -l < m < l\}.$$

Then the normalized displacement field can be expanded in terms of spherical harmonics as below:

$$u(\boldsymbol{\theta},\boldsymbol{\phi}) = \sum_{(l,m)\in\mathcal{K}_N} u_{l,m}Y_{l,m} \tag{7}$$

where Y_{lm}[4] are spherical harmonics (Stein and Weiss, 1971) with eigenvalues:

$$\nabla^2 Y_{l,m} = -q_{l,m}^2 Y_{l,m} = -l(l+1)Y_{l,m}, \tag{8}$$

[3] The surface operators are defined as:

$$\overline{\nabla} := \frac{\partial}{\partial\theta}\mathbf{e}_\theta + \frac{1}{\sin\theta}\frac{\partial}{\partial\phi}\mathbf{e}_\phi, \qquad \underline{\Delta} := \frac{1}{\sin\theta}\frac{\partial}{\partial\theta}\left(\sin\theta\frac{\partial}{\partial\theta}\right) + \frac{1}{\sin^2\theta}\frac{\partial^2}{\partial\phi^2}$$

[4] We have excluded the modes corresponding to $l = 0$ and $l = 1$, since these modes represent the area change and the rigid body motion of the vesicle and hence do not contribute to the total energy. We also recall the two important properties of the spherical harmonics which will be used later in our calculations. They are orthonormal:

$$\int_{\mathbb{S}} Y_{lm}Y_{l'm'}^* d\Omega = \delta_{ll'}\delta_{mm'} \qquad \text{and separable} \qquad Y_{lm} = P_l^m(\theta)e^{im\phi},$$

where $P_l^m(\theta)$ is the Legendre polynomial corresponding to the mode (l,m). In what follows, for the eigenvalues of the spherical harmonics, we use the notation $\mathbf{q} = q_{l,m}$ wherein $\mathbf{q}^2 = q_{l,m}^2 = l(l+1)$.

and $u_{l,-m} = u^*_{l,m}$ are the Fourier transformation of $u(\theta, \phi)$:

$$u_{l,m} = \int_{\mathbb{S}} u(\theta,\phi) Y^*_{lm} d\Omega. \tag{9}$$

Then the total energy in Fourier space can be expanded as:

$$F^{tot} = 4\pi \sum_{(l,m)\in\mathcal{K}_N} \frac{1}{2}(\overline{\kappa} q^4_{l,m} + \overline{\sigma} q^2_{l,m} + \overline{\gamma})|u_{l,m}|^2, \tag{10}$$

where

$$\overline{\kappa} = \frac{1}{4}\kappa_b, \qquad \overline{\sigma} = \sigma r_0^2 - \frac{3}{2}\kappa_b, \qquad \overline{\gamma} = \gamma_d + 2\sigma r_0^2. \tag{11}$$

The partition function and the free energy of the vesicle are then obtained as:

$$\begin{aligned} \mathcal{Z} &= \int_{-\infty}^{\infty} \exp\left(-F^{tot}/k_B T\right) \mathcal{D}[u] = \prod_{q_{l,m}\in\mathcal{K}_N} \sqrt{\frac{k_B T}{2(\overline{\kappa} q^4_{l,m} + \overline{\sigma} q^2_{l,m} + \overline{\gamma})}}, \\ \mathcal{F} &= -k_B T \log \mathcal{Z} = C_{\mathcal{F}} + k_B T \sum_{q_{l,m}\in\mathcal{K}_N} \log\left(\overline{\kappa} q^4_{l,m} + \overline{\sigma} q^2_{l,m} + \overline{\gamma}\right), \end{aligned} \tag{12}$$

where $C_{\mathcal{F}}$ is a constant of no consequences. Up to this point, we have not assigned any value to the potential energy parameter γ_d, (and thus $\overline{\gamma}$). In the next step, we *tune* this parameter such that the out-of-plane fluctuations remain smaller than the distance between two vesicles, i.e. $\langle u^2\rangle < d^2/r_0^2$, where d is the distance between two membranes, $d = R_0 - r_0$. We start with converting this inequality to an equation using a constant, $\delta < 1$:

$$\langle u^2\rangle := \delta \frac{d^2}{r_0^2}, \tag{13}$$

from which the *tuning* parameter γ_d, will be obtained. The fluctuations of the normalized displacement field in Fourier space can be obtained using the equipartition theorem:

$$\langle |u_{l,m}|^2\rangle = \frac{k_B T}{4\pi(\overline{\kappa} q^4_{l,m} + \overline{\sigma} q^2_{l,m} + \overline{\gamma})}, \tag{14}$$

from which the fluctuations in real space is obtained as[5]:

$$\begin{aligned} \langle u^2\rangle &= \sum_{q_{l,m}} \langle |u_{l,m}|^2\rangle = \sum_{q_{l,m}} \frac{k_B T}{4\pi(\overline{\kappa} q^4_{l,m} + \overline{\sigma} q^2_{l,m} + \overline{\gamma})} \\ &= \int_{l_{min}}^{l_{max}} \frac{k_B T (2l+1) dl}{4\pi(\overline{\kappa} l^2 (l+1)^2 + \overline{\sigma} l(l+1) + \overline{\gamma})} = \frac{2k_B T}{\sqrt{4\overline{\gamma\kappa} - \overline{\sigma}^2}} \text{Arctan}\left(\frac{2\overline{\kappa} l(l+1) + \overline{\sigma}}{\sqrt{4\overline{\gamma\kappa} - \overline{\sigma}^2}}\right)\Bigg|_{l_{min}}^{l_{max}} \end{aligned} \tag{15}$$

in which $l_{min} = 2$ and $l_{max} = 4\pi r_0^2/t^2$, where t is the length of the shortest wavelength fluctuations and is typically in the same order of magnitude as the thickness of the membrane. The analytical solution in Eq. (15), depends on the sign of $4\overline{\gamma\kappa} - \overline{\sigma}^2$. Thus, in the following, we consider two cases where this expression is positive and negative.

- **Case I:** $\frac{\overline{\sigma}^2}{4\overline{\gamma\kappa}} \ll 1$.
  This case, corresponds to the condition where either the effective surface tension $\overline{\sigma}$ is quite small or the potential energy parameter $\overline{\gamma}$ is large. In this case, the fluctuations in real space remain the same expression as in (15). Considering that the radius of the vesicle is much larger than its thickness, i.e. $l_{max} \to \infty$, we have:

  $$\langle u^2\rangle = \frac{k_B T \theta}{\sqrt{4\overline{\gamma\kappa} - \overline{\sigma}^2}}, \tag{16}$$

  where $\theta = \pi - 2\text{Arctan}\left(\frac{12\overline{\kappa}+\overline{\sigma}}{\sqrt{4\overline{\gamma\kappa}-\overline{\sigma}^2}}\right)$ is just a constant with no consequences. Then, using the Eq. (13), one can obtain the following expression for γ_d:

  $$\gamma_d = \frac{(k_B T)^2 \theta^2 r_0^4}{\delta^2 \kappa_b d^4} + C_1, \tag{17}$$

  where $C_1 = \frac{9}{4}\kappa_b + r_0^4\sigma^2/\kappa_b - 5r_0^2\sigma$. We now proceed to the second case.

[5] Note that the integral expression serves as an approximation to the discrete summation. While this approximation is reasonably accurate for large vesicles where $t/r_0 \to 0$, it becomes less reliable for smaller vesicles, where the discreteness of the modes plays a more significant role.

- **Case II:** $\frac{\overline{\sigma}^2}{4\overline{\gamma\kappa}} \gg 1$

This case corresponds to the condition where either the surface tension is large or the confinement is small for which the potential energy parameter $\overline{\gamma}$ is small. In this case, the fluctuations in real space is obtained as:

$$\langle u^2 \rangle = \frac{k_B T}{\sqrt{\overline{\sigma}^2 - 4\overline{\gamma\kappa}}} \log\left(\frac{12\overline{\kappa} + \overline{\sigma} + \sqrt{\overline{\sigma}^2 - 4\overline{\gamma\kappa}}}{12\overline{\kappa} + \overline{\sigma} - \sqrt{\overline{\sigma}^2 - 4\overline{\gamma\kappa}}} \right). \tag{18}$$

Substituting (18) into Eq. (13), gives us a nonlinear equation for γ_d, for which an exact analytical solution cannot be found. Yet, the leading terms in the solution for γ_d can be expressed as:

$$\begin{aligned} \gamma_d &\sim \frac{\left(3\kappa_b + 2\sigma r_0^2\right)^2}{4\kappa_b} \mathrm{Sech}^2\left(\frac{d^2\delta\left(2r_0^2\sigma - 3\kappa_b\right)}{4k_B T r_0^2} \right) - 8\sigma r_0^2 \\ &\sim \frac{\left(3\kappa_b + 2\sigma r_0^2\right)^2}{4\kappa_b} \exp\left(-\frac{d^2\delta\left(2r_0^2\sigma - 3\kappa_b\right)}{2k_B T r_0^2} \right) - 8\sigma r_0^2. \end{aligned} \tag{19}$$

In the following, we will use the expressions obtained for the potential energy parameter γ_d to obtain the entropic pressure on the fluctuating vesicle surface, due to the external confinement.

3. Entropic pressure near a fluctuating vesicle surface

Entropic pressure refers to the pressure exerted on the membrane surface due to the presence of external confinements. Similar to the entropic behavior of an ideal gas, when the available volume (V) for the motion of the membrane decreases, the free energy, $\mathcal{F}$ of the system increases. This leads to an increase in the pressure in the system. For a vesicle of radius r_0 confined within a larger vesicle of radius R_0, the available volume for the fluctuations is given by the volume of the outer vesicle, i.e., $V = \frac{4}{3}\pi R_0^3$. In this setup, we assume that the radius of the inner vesicle remains fixed, while the outer vesicle can vary in size, thereby adjusting the confinement gap $d = R_0 - r_0$. The variation of the volume is then given by: $\partial V = 4\pi R_0^2 \partial d$, from which the entropic pressure is derived as:

$$p = -\frac{\partial \mathcal{F}}{\partial V} = -\frac{1}{4\pi R_0^2}\frac{\partial \mathcal{F}}{\partial d} = -\frac{1}{4\pi R_0^2}\frac{\partial \mathcal{F}}{\partial \gamma_d}\frac{\partial \gamma_d}{\partial d}. \tag{20}$$

We will now proceed to derive expressions for entropic pressure for the two different cases discussed in Section 2. Starting with the first case, where the membrane surface tension is small, and/or the confinement distance d is small leading to larger values of potential energy parameter γ_d, the entropic pressure p^s is obtained by substituting Eq. (17) into (20):

$$p^s = -\frac{1}{4\pi R_0^2}\frac{\partial \mathcal{F}}{\partial \gamma_d}\frac{\partial \gamma_d}{\partial d} = \frac{4\langle u^2 \rangle}{R_0^2}\frac{(k_B T)^2\theta^2 r_0^4}{\delta^2 \kappa_b d^5} = \left(\frac{4(k_B T)^2\theta^2 r_0^2}{\delta R_0^2 \kappa_b} \right)\frac{1}{d^3}, \tag{21}$$

where we used the expression for the fluctuations $\langle u^2 \rangle = \delta d^2 / r_0^2$ to calculate the entropic pressure. This power law is the same as that of a tension-less planar membrane and indicates that the power law for the entropic pressure is not affected by the membrane's surface tension when the confining distance d is small, regardless of the shape or curvature of the membrane.

For the second case, where the surface tension is large and/or the confining distance d is large leading to smaller values for the potential energy parameter γ_d, the entropic pressure p^l can be obtained by substituting Eq. (19) into (20) as:

$$\begin{aligned} p^l &= -\frac{1}{4\pi R_0^2}\frac{\partial \mathcal{F}}{\partial \gamma_d}\frac{\partial \gamma_d}{\partial d} = \left(\frac{\langle u^2 \rangle}{R_0^2} \right)\frac{d\delta\left(2r_0^2\sigma - 3\kappa_b\right)\left(3\kappa_b + 2r_0^2\sigma\right)^2}{4r_0^2\kappa_b k_B T}\exp\left(-\frac{d^2\delta\left(2r_0^2\sigma - 3\kappa_b\right)}{2r_0^2 k_B T} \right) \\ &= \left(\frac{\delta d^2}{r_0^2 R_0^2} \right)\frac{d\delta\left(2r_0^2\sigma - 3\kappa_b\right)\left(3\kappa_b + 2r_0^2\sigma\right)^2}{4r_0^2\kappa_b k_B T}\exp\left(-\frac{d^2\delta\left(2r_0^2\sigma - 3\kappa_b\right)}{2r_0^2 k_B T} \right) \\ &= \frac{d^3\delta^2\left(2r_0^2\sigma - 3\kappa_b\right)\left(3\kappa_b + 2r_0^2\sigma\right)^2}{4r_0^4 R^2\kappa_b k_B T}\exp\left(-\frac{d^2\delta\left(2r_0^2\sigma - 3\kappa_b\right)}{2r_0^2 k_B T} \right) \sim f d^3 \exp\left(-\alpha d^2\right), \end{aligned} \tag{22}$$

where we have simplified the final result to highlight the exponential decaying trend of the entropic pressure. The coefficients f and α are just constants in the final form and as can be seen in Eq. (22), depend on the mechanical properties, the radii of the inner and outer vesicles and the temperature. Eq. (22) shows that the effective surface tension that depends on the curvature of the vesicle affects the power law for entropic pressure at larger confining distances d.

In the following section, we aim to validate our predictions with molecular dynamics simulations.

4. Molecular dynamics simulations of the entropic force near a fluctuating membrane with surface tension

In this section we aim to study the entropic force on a fluctuating membrane with surface tension via a coarse-grained molecular dynamics model. Recognizing that the confined fluctuations of the vesicle described in Eq. (14) are equivalent to those of a planar membrane with renormalized properties $\overline{\kappa}$, $\overline{\sigma}$, and $\overline{\gamma}_d$, confined between two hard walls separated by a distance $2d = 2(R_0 - r_0)$, we

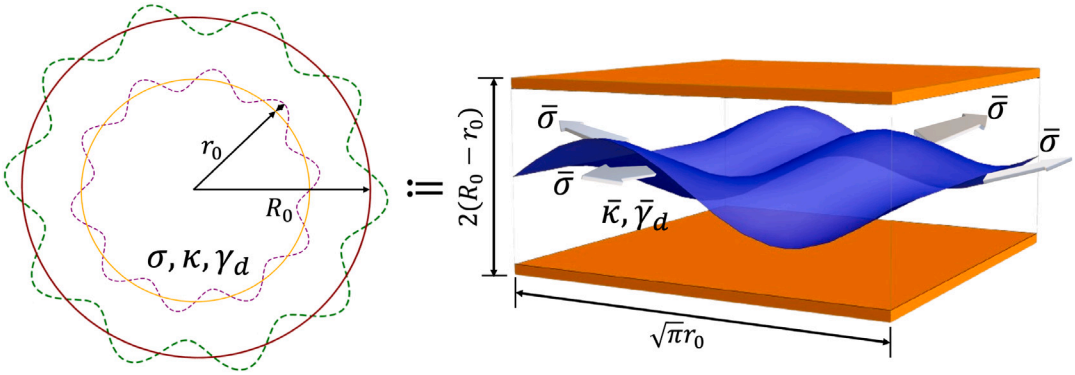

Fig. 4. Schematic of the analogy between the fluctuations in a vesicle, Eq. (14) with those of a planar membrane, having renormalized properties.

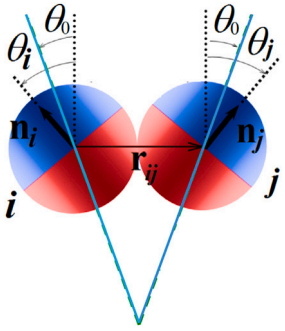

Fig. 5. Schematic representation of the anisotropic interparticle potential employed in the one-particle-thick, solvent-free coarse-grained membrane model (Yuan et al., 2010a). Each particle symbolizes a lipid cluster, interacting through a pair potential modulated by their relative orientations—see Eq. (23).
Source: The picture is adapted from Yuan et al. (2010a).

will perform simulations on a planar membrane with these adjusted properties. For the vesicle, although the curvature field induces a negative surface tension in the membrane, we included an additional surface tension term in the elastic energy (Eq. (2)) to ensure that the coefficient of the q^2 term remains strictly positive, thereby maintaining the stability of the vesicle. With this formulation, the effective surface tension exhibits a noticeable variation *only* at large q values, corresponding to modes with smaller amplitude fluctuations. This approach effectively captures the entropic behavior of a vesicle while simplifying the complexities associated with simulating interactions between large vesicles. A schematic of this analogy is demonstrated in Fig. 4.

4.1. Coarse grained model of lipid vesicle

In our molecular dynamics simulations, we employed a highly coarse-grained, one-particle-thick, solvent-free lipid membrane model (Yuan et al., 2010a; Fu et al., 2017). In this model, each lipid molecule is represented by a single spherical particle, encompassing both translational and rotational degrees of freedom. Consequently, the interactions between lipid particles are influenced by their relative distances and orientations.

4.2. Pair-potential model for vesicle

In our model, the interparticle potential comprises two functions, $U(r)$ and $\phi(\hat{r}_{ij}, n_i, n_j)$, which respectively describe the distance and orientation dependencies. The interactions between lipid particles are described by the following potentials:

$$U(r_{ij}, n_i, n_j) = \begin{cases} U_R(r) + \left(1 - \phi(\hat{r}_{ij}, n_i, n_j)\right)\epsilon, & \text{if } r < r_{\min} \\ U_A(r)\phi(\hat{r}_{ij}, n_i, n_j), & \text{if } r_{\min} \le r < r_c \end{cases} \tag{23}$$

where $U_R(r)$ and $U_A(r)$ are the distance-dependent repulsive and attractive potentials, respectively, $r_{\min}$ is the repulsive force range, and r_c is the cutoff distance of the pair-wise interaction. The function $\phi(\hat{r}_{ij}, n_i, n_j)$ is an angular function to tune the interaction force based on the relative orientation between particle pair r_i and r_j, where $\hat{r}_{ij} = \frac{r_{ij}}{r}$ is the vector direction of the relative distance vector r_{ij} between two particles, and n_i and n_j represent the orientation of particles i and j, respectively (Yuan et al., 2010a; Fu et al., 2017). The distance dependent repulsive $U_R(r)$ and attractive $U_A(r)$ potentials are:

$$U_R(r) = \epsilon\left(\left(\frac{r_{\min}}{r}\right)^4 - 2\left(\frac{r_{\min}}{r}\right)^2\right), \quad r < r_{\min} \tag{24}$$

$$U_A(r) = -\epsilon \left(\cos\left(\frac{\pi(r - r_{\min})}{2(r_c - r_{\min})} \right) \right)^{2\xi}, \quad r_{\min} \le r < r_c \tag{25}$$

Here, ϵ and s are the energy and length units, respectively. The repulsive part $U_R(r)$ is modeled by a 4-2 Lennard-Jones potential. The attractive branch $U_A(r)$ follows a cosine function that smoothly decays to zero at the cutoff distance r_c. The exponent ξ adjusts the slope of the attractive branch, thereby tuning particle diffusivity. The branches meet smoothly at $r = r_{\min}$ with C^1 continuity. We set the distance at the minimum of the potential $r_{\min} = \sqrt[6]{2}s$ and $r_c = 2.6s$ to incorporate second-neighbor interactions.

The orientation-dependent function ϕ modifies the potential by scaling the attractive branch of the distance-dependent interaction and shifting the repulsive branch upward. This adjustment ensures a consistent minimum energy distance regardless of the relative orientations between two particles. Representing hydrophobic effects, the function ϕ is defined as:

$$\phi = 1 + \mu \left[a(\hat{r}_{ij}, n_i, n_j) - 1 \right]$$

where

$$a = (\hat{n}_i \times \hat{r}_{ij}) \cdot (\hat{n}_j \times \hat{r}_{ij}) - \sin\theta_0 (\hat{n}_j - \hat{n}_i) \cdot \hat{r}_{ij} - \sin^2\theta_0$$

The function a (and thus ϕ) reaches its maximum value of 1 when the angle between two particles is θ_0 and is less than 1 otherwise. A schematic of these variables is shown in Fig. 5.

Further details about the model can be found in Fu et al. (2017) and Yuan et al. (2010a). We chose typical parameters of $\epsilon = 1$, $s = 1$, $r_c = 2.6$, $\xi = 4$, $\mu = 3$, and $\theta_0 = 0$ at a temperature of $T = 0.23\frac{\epsilon}{k_B}$. The mass of each particle is set to unity, and the time scale is defined as $\tau = \sqrt{\frac{\epsilon}{ms^2}}$.

4.3. Interaction between the fluctuating membrane and the confining walls

To accurately simulate the steric effect of the lipid membrane confined between two hard walls (Fig. 4), a short-ranged repulsive force is implemented between lipid particles and the confining walls. This force becomes significant when the distance between the lipid particles and the walls falls within a specified cutoff distance (r_{cut}). In out model, we use the popular Weeks–Chandler–Anderson (WCA) potential,

$$\varphi(r) = \begin{cases} 4\epsilon \left(\left(\frac{s}{r}\right)^{12} - \left(\frac{s}{r}\right)^{6} \right) + \epsilon, & r \le 2^{1/6}s \\ 0, & r > 2^{1/6}s \end{cases}$$

where r is the distance between the lipid particle and the confining wall, with $r_{\text{cut}} = \frac{2^{1/6}s}{\epsilon}$. The code for command fix wall/lj126 in LAMMPS was modified to implement this potential. This potential is the Lennard-Jones (LJ) potential, shifted upwards by ϵ and truncated at the LJ potential minimum of $r = 2^{1/6}s$. While the total potential remains repulsive, it comprises both repulsive (r^{-12}) and attractive (r^{-6}) interactions.

4.4. Simulation protocol and results

In our simulations, the system comprised 108,900 particles in a simulation box extending from $-150s$ to $150s$ in the x and y directions, and from $-50s$ to $50s$ in the z direction. This configuration results in a system size of $300s$ in the x and y directions, and $100s$ in the z direction. The time step is set at $\Delta t = 0.005\tau$. The simulation protocol began with the NVT ensemble, employing a Nose–Hoover thermostat to maintain the temperature at $T = 0.23\frac{\epsilon}{k_B}$, which has been suggested for the one-particle lipid model (Yuan et al., 2010a,b). The membrane was then stretched to different strains with the strain rate of $1 \times 10^{-4}\,\tau^{-1}$. For example, to achieve the strain of 4%, the simulation times for the stretching step is $400\,\tau$. Following that, the membrane was confined within two walls with a wall-membrane distance d.

Prior to computing the entropic force, molecular dynamics simulations were performed on the membrane in the absence of confinement, using the NVT ensemble. The resulting fluctuation spectrum revealed that the coarse-grained membrane model exhibits an intrinsic compressive stress, which manifests as an effective negative surface tension due to the fixed projected area. When a biaxial strain of 2% was applied in both the x- and y-directions, this preexisting surface tension was effectively neutralized, and the fluctuation spectrum recovered the characteristic $1/q^4$ scaling of a tensionless membrane. The results of the fluctuation spectra for membranes subjected to four different strain levels–2%, 3%, 4%, and 5%–are presented in Fig. 6. At a strain of 3%, the fluctuation spectrum shows a slight deviation from the $1/q^4$ scaling, indicating the presence of a small but finite surface tension. However, this surface tension is not sufficient to drive the system into the tension-dominated regime, which is characterized by a $1/q^2$ scaling. For higher strain values, including 4% and 5%, the fluctuation spectrum clearly reflects the onset of a positive surface tension, with a dominant contribution characteristic of a tension-governed regime.

Different wall-membrane distances, varying from $5.5s$ to $11s$, were implemented to confine the membrane and induce membrane fluctuations. The illustration of the membrane fluctuation is shown in Fig. 7 (right), with color coding referring to the out-of-plane fluctuations of the particles. For each confining distance d, the simulations were run for $3.0 \times 10^4\tau$, sufficiently long for the entropic force to converge. The total force was recorded every 5τ and averaged over the last $1.5 \times 10^4\tau$. All simulations were conducted using the LAMMPS software (Plimpton, 1995).

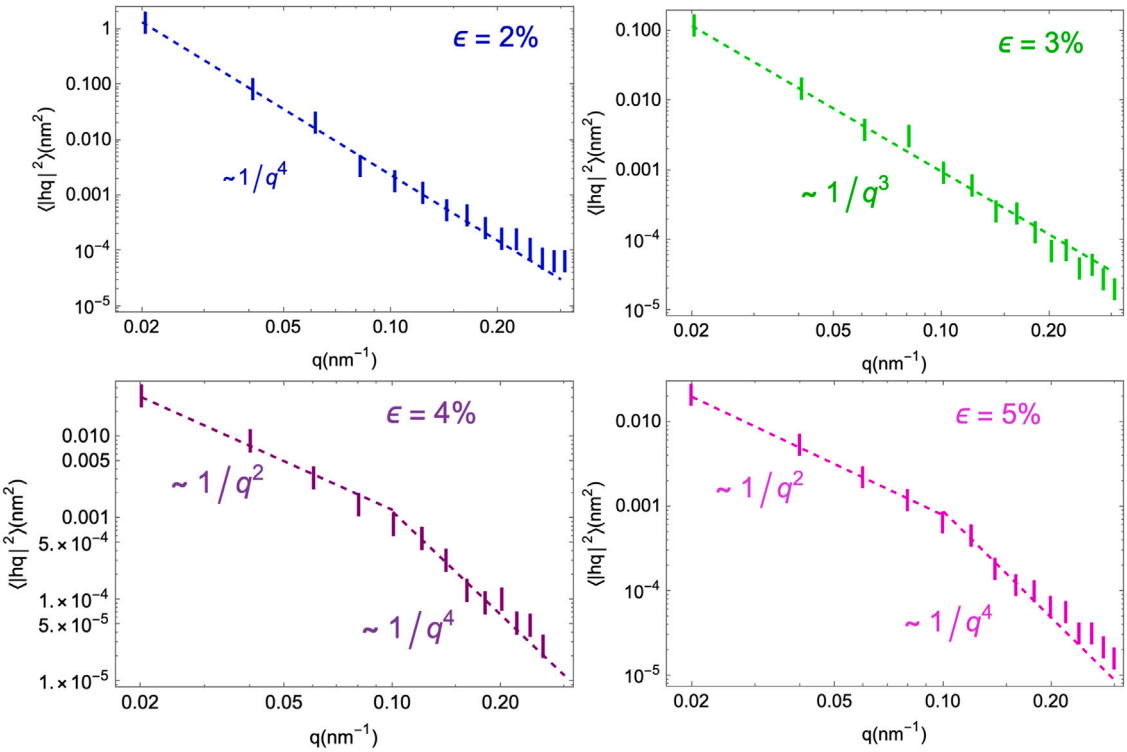

Fig. 6. Fluctuation spectra for a membrane of size $300s$ in the coarse-grained molecular dynamics simulations. Strains were applied simultaneously in both x and y directions. The simulations were performed under NVT ensemble, where the simulation box size can be assigned and fixed while pressure can vary to reach equilibrium state. Under these conditions, the coarse-grained model of the fluctuating membrane exhibits an intrinsic compressive stress, manifested as an effective negative surface tension. Our results indicate that applying an in-plane strain of approximately 2% is sufficient to relax this preexisting compressive stress. At this strain, the membrane's fluctuation spectra recovers the tensionless form, characterized by the scaling $\langle|h_q|^2\rangle \sim 1/q^4$. At a strain of 3%, the fluctuation spectrum exhibits a slight deviation from the $1/q^4$ scaling, indicating the emergence of a small but finite surface tension. However, this tension remains insufficient to shift the spectral scaling to the tension-dominated regime characterized by $1/q^2$. For higher strain values, including 4% and 5%, the fluctuation spectrum clearly reflects the onset of a positive surface tension, with a dominant contribution characteristic of a tension-governed regime.

The results of the coarse-grained MD simulations of the entropic force at different wall-membrane distances are illustrated in Fig. 7 (left). Based on the fluctuation spectra, we find that a strain of 2%, which corresponds to vanishing surface tension, yields an entropic pressure consistent with the scaling law for a tensionless membrane, namely $p \sim 1/d^3$. As the strain increases to 3%, the fluctuation spectrum begins to deviate slightly from the tensionless case, suggesting the emergence of a small but finite positive surface tension. In this intermediate regime, the entropic pressure exhibits a modified scaling behavior, and the best fit to the data reveals a power-law decay of $p \sim 1/d^{2.3}$. For higher strains of 4% and 5%, the fluctuation spectra indicate a pronounced surface tension. The corresponding MD results for entropic pressure, shown in Fig. 7, display an exponential decay, $p \propto f d^3 \exp(-\alpha d^2)$, consistent with our theoretical predictions for tension-dominated membranes.

5. Summary and conclusion

In this study, we have provided a comprehensive analysis of the fluctuations of vesicle with surface tension, confined within a larger vesicle. Such confinement results in entropic force exerted on both vesicles, hindering their fusion and is crucial for the stability of multilamellar and multivesicular biological structures. While this topic has been addressed in the past for the case of planar membrane without surface tension, it has not been studied for curved fluctuating surfaces where the fluctuations are coupled with the existing curvature field. This geometrical coupling results in renormalizing the surface tension of the membrane and even in the absence of the surface tension, impacts the scaling law for the entropic force. Our results are summarized as follow:

- We developed a statistical mechanics model of a confined fluctuating vesicle to study the entropic force near a curved fluctuating surface. At close distance and with small values of surface tension the scaling is similar to that of a planar membrane and the entropic pressure varies as $p \propto 1/d^3$. At larger distance and/or with larger values of surface tension however, the scaling law changes and becomes exponentially decaying, i.e. $p \propto d^3 \exp(-f d^2)$. This trend also applies to a planar membrane with surface tension, yet for a curved surface even without surface tension, the entropic pressure decays exponentially due to the presence of an existing curvature field.

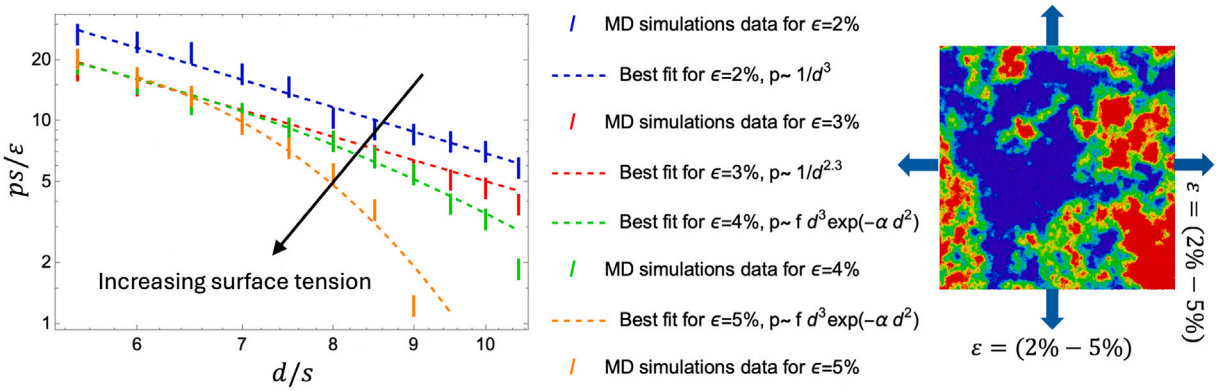

Fig. 7. (Left) Results from the coarse-grained molecular dynamics simulations on the entropic force at different wall distances. Based on the fluctuation spectra, we find that a strain of 2%, which corresponds to vanishing surface tension, results in an entropic pressure consistent with the expected scaling for a tensionless membrane, namely $p \sim 1/d^3$. As the strain is increased to 3%, the fluctuation spectrum exhibits a slight deviation from this scaling, indicating the onset of a small but finite positive surface tension. In this intermediate regime, the entropic pressure follows a modified power-law behavior, with the best fit yielding $p \sim 1/d^{2.3}$. For higher strains of 4% and 5%, the fluctuation spectra clearly demonstrate significant surface tension. The corresponding MD results for the entropic pressure reveal an exponential decay of the form $p \propto f d^3 \exp(-\alpha d^2)$, in excellent agreement with our theoretical predictions for membranes in the tension-dominated regime. (Right) Top view of the fluctuating membrane under stretch in the coarse-grained molecular dynamics simulation. The out-of-plane displacement function of the particles is color-coded.

- Our theoretical predictions are supported by a series of coarse-grained MD simulations. To clearly capture entropic effects, it is essential to consider membranes large enough to exhibit appreciable thermal fluctuations. All-atom simulations, however, are computationally inefficient for such large-scale systems. Noting that the fluctuation behavior of a vesicle resembles that of a planar membrane with *renormalized* elastic properties, we modeled a planar membrane using effective bending rigidity and surface tension parameters. This strategy significantly reduced computational complexity while capturing the essential physics of vesicle confinement. To induce surface tension, we applied a range of in-plane strains–2%, 3%, 4%, and 5%–and computed the force on rigid walls placed at varying distances from the membrane. Not all strain values led to finite surface tension. The presence or absence of surface tension was verified by analyzing the fluctuation spectra of unconfined membranes under each strain condition. As shown in Fig. 6, the 2% strain case corresponds to a tensionless membrane, 3% induces a small positive surface tension, while 4% and 5% lead to significant surface tension. The resulting entropic pressure data are presented in Fig. 7, and demonstrate excellent agreement with the theoretical expression given in Eq. (22).
- While the theoretical framework developed here is broadly applicable to any fluid membrane, the specific results obtained from the computational model depend strongly on the choice of interatomic potentials and the level of coarse-graining employed. In this study, our focus has been limited to a qualitative comparison between the theoretical predictions and simulation results. A rigorous quantitative comparison would require all-atom simulations with well-characterized mechanical properties – such as the bending modulus and surface tension – which is beyond the scope of the present work.

A comprehensive exploration of the biological implications of our calculations is beyond the scope of this work. However, we anticipate that our findings will be relevant to many of the phenomena discussed in the introduction of this paper. The impact of our work on these problems remains to be determined.

CRediT authorship contribution statement

Rubayet Hassan: Validation, Investigation, Formal analysis. **Mingze Cai:** Methodology, Data curation. **Anh Vo:** Investigation, Formal analysis, Data curation. **Samaneh Farokhirad:** Writing – review & editing, Funding acquisition. **Xin Yan:** Writing – review & editing, Supervision, Methodology, Conceptualization. **Fatemeh Ahmadpoor:** Writing – original draft, Validation, Supervision, Project administration, Funding acquisition, Formal analysis, Conceptualization.

Declaration of competing interest

The authors declare the following financial interests/personal relationships which may be considered as potential competing interests: Fatemeh Ahmadpoor reports financial support was provided by National Science Foundation. Samaneh Farokhirad reports financial support was provided by National Science Foundation. If there are other authors, they declare that they have no known competing financial interests or personal relationships that could have appeared to influence the work reported in this paper.

Acknowledgment

Fatemeh Ahmadpoor and Samaneh Farokhirad gratefully acknowledge financial support from the New Jersey Institute of Technology and the National Science Foundation, United States through Grants No. CMMI-2237530 and CBET-2327899.

Data availability

Data will be made available on request.

References

Abbena, E., Salamon, S., Gray, A., 2006. Modern Differential Geometry of Curves and Surfaces with Mathematica. CRC Press.

Ahmadpoor, F., Sharma, P., 2016a. A perspective on the statistical mechanics of 2d materials. Extreme Mech. Lett..

Ahmadpoor, F., Sharma, P., 2016b. Thermal fluctuations of vesicles and nonlinear curvature elasticity—implications for size-dependent renormalized bending rigidity and vesicle size distribution. Soft Matter 12 (9), 2523–2536.

Ahmadpoor, F., Zou, G., Gao, H., 2022. Entropic interactions of 2d materials with cellular membranes: Parallel versus perpendicular approaching modes. Mech. Mater. 174, 104414.

Bachmann, M., Kleinert, H., Pelster, A., 2001. Fluctuation pressure of a stack of membranes. Phys. Rev. E 63 (5), 051709.

Biria, A., Maleki, M., Fried, E., 2013. Continuum theory for the edge of an open lipid bilayer. Adv. Appl. Mech. 21, 1–78.

Chen, W., Evans, E.A., McEver, R.P., Zhu, C., 2008. Monitoring receptor–ligand interactions between surfaces by thermal fluctuations. Biophys. J. 94 (2), 694–701.

Chen, D., Kulkarni, Y., 2015. Entropic interaction between fluctuating twin boundaries. J. Mech. Phys. Solids 84, 59–71.

Chen, D., Kulkarni, Y., 2017. Thermal fluctuations as a computational microscope for studying crystalline interfaces: A mechanistic perspective. J. Appl. Mech. 84 (12).

Dearnley, M., Chu, T., Zhang, Y., Looker, O., Huang, C., Klonis, N., Yeoman, J., Kenny, S., Arora, M., Osborne, J.M., et al., 2016. Reversible host cell remodeling underpins deformability changes in malaria parasite sexual blood stages. Proc. Natl. Acad. Sci. 113 (17), 4800–4805.

Farokhirad, S., Bradley, R.P., Radhakrishnan, R., 2019. Thermodynamic analysis of multivalent binding of functionalized nanoparticles to membrane surface reveals the importance of membrane entropy and nanoparticle entropy in adhesion of flexible nanoparticles. Soft Matter 15 (45), 9271–9286.

Farokhirad, S., Kandy, S.K., Tsourkas, A., Ayyaswamy, P.S., Eckmann, D.M., Radhakrishnan, R., 2021. Biophysical considerations in the rational design and cellular targeting of flexible polymeric nanoparticles. Adv. Mater. Interfaces 8 (23), 2101290.

Freund, L., 2013. Entropic pressure between biomembranes in a periodic stack due to thermal fluctuations. Proc. Natl. Acad. Sci. 110 (6), 2047–2051.

Fu, S.-P., Peng, Z., Yuan, H., Kfoury, R., Young, Y.-N., 2017. Lennard-jones type pair-potential method for coarse-grained lipid bilayer membrane simulations in lammps. Comput. Phys. Comm. 210, 193–203.

Gao, H., Shi, W., Freund, L.B., 2005. Mechanics of receptor-mediated endocytosis. Proc. Natl. Acad. Sci. 102 (27), 9469–9474.

Gov, N., Zilman, A., Safran, S., 2003. Cytoskeleton confinement and tension of red blood cell membranes. Phys. Rev. Lett. 90 (22), 228101.

Gruner, S.M., Lenk, R.P., Janoff, A.S., Ostro, N.J., 1985. Novel multilayered lipid vesicles: comparison of physical characteristics of multilamellar liposomes and stable plurilamellar vesicles. Biochemistry 24 (12), 2833–2842.

Hanlumyuang, Y., Liu, L., Sharma, P., 2014. Revisiting the entropic force between fluctuating biological membranes. J. Mech. Phys. Solids 63, 179–186.

Hassan, R., Garzon, M.A., Gao, W., Ahmadpoor, F., 2024. Entropic pressure on fluctuating solid membranes. J. Mech. Phys. Solids 183, 105523.

Helfrich, W., 1973. Elastic properties of lipid bilayers: theory and possible experiments. Z. Nat. C 28 (11–12), 693–703.

Helfrich, W., 1978. Steric interaction of fluid membranes in multilayer systems. Z. Nat. A 33 (3), 305–315.

Helfrich, W., 1986. Size distributions of vesicles: the role of the effective rigidity of membranes. J. Physique 47 (2), 321–329.

Huang, C., Quinn, D., Sadovsky, Y., Suresh, S., Hsia, K.J., 2017. Formation and size distribution of self-assembled vesicles. Proc. Natl. Acad. Sci. 114 (11), 2910–2915.

Kalluri, R., LeBleu, V.S., 2020. The biology, function, and biomedical applications of exosomes. Science 367 (6478), eaau6977.

Kleinert, H., 1999. Fluctuation pressure of membrane between walls. Phys. Lett. A 257 (5), 269–274.

Kulkarni, Y., 2023. Fluctuations of active membranes with nonlinear curvature elasticity. J. Mech. Phys. Solids 173, 105240.

Kusters, R., Simon, C., Dos Santos, R.L., Caorsi, V., Wu, S., Joanny, J.-F., Sens, P., Sykes, C., 2019. Actin shells control buckling and wrinkling of biomembranes. Soft Matter 15 (47), 9647–9653.

Laplace, P.-S., 1806. Mécanique Céleste, vol. 4, Chez Courcier, Paris, Original work in French.

Lee, J.-H., Choi, S.-M., Doe, C., Faraone, A., Pincus, P.A., Kline, S.R., 2010. Thermal fluctuation and elasticity of lipid vesicles interacting with pore-forming peptides. Phys. Rev. Lett. 105 (3), 038101.

Liang, X., Purohit, P.K., 2018. A method to compute elastic and entropic interactions of membrane inclusions. Extrem. Mech. Lett. 18, 29–35.

Lipowsky, R., 1991. The conformation of membranes. Nature 349 (6309), 475–481.

Lipowsky, R., Leibler, S., 1986. Unbinding transitions of interacting membranes. Phys. Rev. Lett. 56 (23), 2541.

Lipowsky, R., Seifert, U., 1991. Adhesion of vesicles and membranes. Mol. Cryst. Liq. Cryst. 202 (1), 17–25.

Loubet, B., Seifert, U., Lomholt, M.A., 2012. Effective tension and fluctuations in active membranes. Phys. Rev. E—Stat. Nonlinear Soft Matter Phys. 85 (3), 031913.

Mamun, S., Farokhirad, S., 2024. Collision dynamics and deformation behaviors of multi-core compound droplet pairs in microchannel flow. arXiv preprint arXiv:2412.07109.

Morse, D.C., Milner, S.T., 1995. Statistical mechanics of closed fluid membranes. Phys. Rev. E 52 (6), 5918.

Mozaffari, K., Ahmadpoor, F., Sharma, P., 2021. Flexoelectricity and the entropic force between fluctuating fluid membranes. Math. Mech. Solids 26 (12), 1760–1778.

Papahadjopoulos, D., Kimelberg, H.K., 1974. Phospholipid vesicles (liposomes) as models for biological membranes: their properties and interactions with cholesterol and proteins. Prog. Surf. Sci. 4, 141–232.

Plimpton, S., 1995. Fast parallel algorithms for short-range molecular dynamics. J. Comput. Phys. 117 (1), 1–19.

Ramesh, S., Kulkarni, Y., 2024. Statistical mechanics of active vesicles and the size distribution paradox. J. Mech. Phys. Solids 191, 105749.

Robbins, P.D., Morelli, A.E., 2014. Regulation of immune responses by extracellular vesicles. Nat. Rev. Immunol. 14 (3), 195–208.

Seifert, U., 1997. Configurations of fluid membranes and vesicles. Adv. Phys. 46 (1), 13–137.

Sharma, P., 2013. Entropic force between membranes reexamined. Proc. Natl. Acad. Sci. 110 (6), 1976–1977.

Sharma, A., Sharma, U.S., 1997. Liposomes in drug delivery: progress and limitations. Int. J. Pharm. 154 (2), 123–140.

Stein, E.M., Weiss, G., 1971. Fourier analysis on euclidean spaces.

Südhof, T.C., 2013. Neurotransmitter release: the last millisecond in the life of a synaptic vesicle. Neuron 80 (3), 675–690.

Sun, T., Zhang, Y.S., Pang, B., Hyun, D.C., Yang, M., Xia, Y., 2021. Engineered nanoparticles for drug delivery in cancer therapy. Nanomater. Neoplasms 3, 1–142.

Turlier, H., Betz, T., 2018. Fluctuations in active membranes. Phys. Biol. Membr. 58, 1–619.

Van Niel, G., d'Angelo, G., Raposo, G., 2018. Shedding light on the cell biology of extracellular vesicles. Nature Rev. Mol. Cell Biol. 19 (4), 213–228.

Weikl, T.R., Lipowsky, R., 2004. Pattern formation during t-cell adhesion. Biophys. J. 87 (6), 3665–3678.

Yamanaka, N., Marqués, G., O'Connor, M.B., 2015. Vesicle-mediated steroid hormone secretion in drosophila melanogaster. Cell 163 (4), 907–919.

Yáñez-Mó, M., Siljander, P.R.-M., Andreu, Z., Bedina Zavec, A., Borràs, F.E., Buzas, E.I., Buzas, K., Casal, E., Cappello, F., Carvalho, J., et al., 2015. Biological properties of extracellular vesicles and their physiological functions. J. Extracell. Vesicles 4 (1), 27066.

Yuan, H., Huang, C., Li, J., Lykotrafitis, G., Zhang, S., 2010a. One-particle-thick, solvent-free, coarse-grained model for biological and biomimetic fluid membranes. Phys. Rev. E 82 (1), 011905.

Yuan, H., Li, J., Bao, G., Zhang, S., 2010b. Variable nanoparticle-cell adhesion strength regulates cellular uptake. Phys. Rev. Lett. 105 (13), 138101.